Chapter 4

The contribution of CHRIS-PROBA multiple view angle data for forest type discrimination *

Abstract

The directional anisotropy of vegetation remote sensing data has been seen as a valuable information source to characterise the vegetation canopy structure. Several studies were devoted to the relationship between the structural characteristics of vegetation canopy and the bidirectional reflectance measured from ground, from air-borne and coarse spatial resolution space-borne sensors. The CHRIS sensor on-board the PROBA satellite has been the first high spatial resolution space-borne sensor dedicated to the acquisition of nearly simultaneous multiple view angle images. In this study, the potential of such data for temperate forest types discrimination was assessed with emphasis on the stand structure. The results showed that most forest types could be discriminated on the basis of near-nadir spectral data alone. However, two deciduous forest types differing essentially by their tree density were discriminable only thanks to off-nadir images. The directional data were therefore a useful complement to the spectral information provided by single view angle images.

*Adapted from Kayitakire, F., Defourny, P., Forest type discrimination using multi-angle hyperspectral data. *Proc. of the 2nd CHRIS/Proba Workshop*, ESA/ESRIN, Frascati, Italy 28-30 April (ESA SP-578, July 2004)

4.1 Introduction

The directional anisotropic behaviour of remotely sensed earth's surface objects has been largely demonstrated. This anisotropy is regarded either as noise to remove from data or as a valuable source of information on the structural features of the sensed objects. Correcting for the directional effects often consists in normalizing the multi-angle reflectances to the nadir view or to a constant "off-nadir" view angle. It is currently applied in the multi-temporal compositing of coarse spatial resolution images acquired by sensors with a large field of view (Leroy and Hautecoeur, 1999; Huete et al., 2002; Duchemin and Maisongrande, 2002). The analysis of spectral data without taking into account the geometric properties of the image acquisition could lead to erroneous conclusions. For example, Deering et al. (1999) showed that the Normalised Difference Vegetation Index (NDVI) values of coniferous stands in a boreal forest might vary considerably (from 0.36 to 0.54) when the view zenith angle (VZA) changed.

On the other hand, structure information of the land cover, e.g. vegetation canopy structure, can be derived from the directional properties of multi-angle images, namely through the bidirectional reflectance distribution function (BRDF) parameters (Gao et al., 2003; Chopping et al., 2003). A review of the application of BRDF models to infer land cover parameters at regional and global scales has been proposed by Roberts (2001). At local scale, e.g. at agricultural parcel or forest stand level, the directional reflectance effects may be a source of valuable information in addition to the spectral and temporal signal (Goel and Reynolds, 1989; Kimes et al., 2006).

Barnsley et al. (1997) assessed the relative contribution of the directional and spectral components to the statistical variance of aerial multiple view angle images taken over an agricultural area. They showed that the spectral component tended to dominate in all wavebands while the directional component explained 3 % to 21 % of the total statistical variance in the near-infrared (NIR) and red wavelengths, respectively. Even if the investigated land cover classes were quite separable on the basis of the spectral content alone in the NIR band, the directional component was still important in discriminating between two classes which exhibited similar spectral signatures in the nadir-viewing image.

The contribution of the directional component was also investigated by Sandmeier and Deering (1999) in deriving forest canopy structure parameters and classifying boreal forests on the basis of air-borne hyperspectral BRDF data. They found that the integration of the BRDF information, through an anisotropy index, substantially increased the overall classification accuracy (from 37.8 % to 44.7 %), but the improvement was not consistent for all classes. For some classes, the producer's accuracy diminished dramatically (from 53.5 % to 22.9 %, and from 47.0 % to 26.1 %) when the BRDF data were included. This raises the question of the usefulness of the anisotropy index used in this study since the class which contributed significantly to the overall accuracy improvement (from 55.4 % to 86.4 %) was a clear peat bog.

Studies on multiple view angles data have been usually carried out using either ground measurements or air-borne sensors data. Only few studies were devoted to near-simultaneous multi-angle data acquired by space-borne sensors. Indeed, apart from the POLDER-1 sensor (Polarization and Directionality of the Earth's Reflectance), on board ADEOS-1 (Advanced Earth Observing Satellite), which operated for 8 months in 1996-1997, the three other really multi-view spaceborne sensors, i.e. POLDER-2, the CHRIS-PROBA system described in section 4.2, and the Multiangle Imaging SpectroRadiometer (MISR) on-board the Terra satellite, are relatively recent. Furthermore, CHRIS-PROBA is the first space-borne sensor to acquire high spatial resolution and near-simultaneous multiple view angle images allowing local studies such as forest stand characterisation. The IKONOS-2, Orbview-3 and QuickBird satellites could also deliver near-simultaneous multiple view angle images for BRDF studies thanks to their great agility but these technical capabilities can hardly be used owing to their high cost.

This study aims, therefore, to investigate the information content in multiple view angle data from a high spatial resolution space-borne sensor for forest type characterisation, with emphasis on directional effect contribution compared to spectral effect. The used data were acquired in the framework of the European Space Agency (ESA) scientific programme of the CHRIS-PROBA mission.

4.2 CHRIS-PROBA system characteristics

The PROBA (PRoject for On Board Autonomy) spacecraft is a mini-satellite (94 Kg) operated by the European Space Agency to explore the feasibility and benefits of autonomy in space. It was launched on October 22^{nd}, 2001. The satellite is capable of along and across-track pointing. The main payload of PROBA is the CHRIS (Compact High Resolution Imaging Spectrometer) sensor which can acquire up to 63 spectral bands (400 nm - 1050 nm) with nominal spatial resolutions of 17 m or 34 m at nadir. The CHRIS sensor can be commissioned from the ground station, allowing different acquisition modes according to the number and location of spectral bands, the spatial resolution and the width of the swath. However, only five principal modes are actually used. They have been selected according to the requirements for four major application fields: aerosol, land cover, vegetation and coastal zones. Thus, the CHRIS-PROBA system allows to acquire hyperspectral images of the same scene with five different view angles during a single overpass. At high latitude ($> 35°$), additional ten images (five image on each side of the principal track) can be captured within three days thanks to the across-track pointing capabilities.

The system acquires the images at times when its zenith angle is approximately equal to a set of so-called Fly-by Zenith Angles (FZA):$+55°$, $+36°$, $0°$, $-36°$ and $-55°$. When the satellite is pointing along-track, the FZA is in that case equivalent to the platform zenith angle. But when the satellite is pointing laterally, the real zenith angle is calculated by considering the FZA with respect

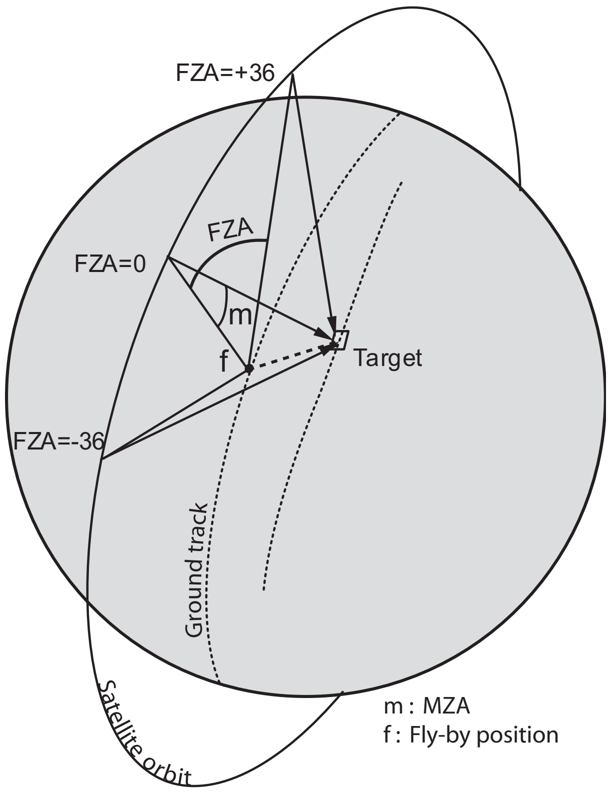

Figure 4.1: Schematic drawing of observation angles of PROBA satellite. We represented only three satellite positions for the clarity of the figure.

to the so-called fly-by position. That is the position on the sub-satellite track at which the platform zenith angle, as seen from the target, is a minimum. This angle, hereafter called the Minimum Zenith Angle (MZA), is equivalent to the roll angle of the 0°–FZA image. Figure 4.1 shows the geometry of observation for three satellite positions: at FZA= +36°, the satellite is pointing forward and across; at FZA= 0°, it is pointing across (note that the MZA is defined at this position), and at FZA= −36°, it is pointing backward and across.

This is however a simple description of the image acquisition process. Actually, the satellite operates on a time basis, and the spatial position of the satellite is approximative when it is pointing to the ground target. The exact position is calculated after the acquisition on the basis of the exact time of the image acquisition and the telemetry data.

In order to minimise the platform movement in pointing manoeuvres, the first image, i.e. the +55°–FZA image, is acquired in synchronous scanning mode (north–south direction) while the second image, i.e. the +36°–FZA image, is acquired in asynchronous scanning mode (south-north direction). Thus, three scans (+55°, 0° and −55°) are executed in north-south direction while the two others (+36° and −36°) are executed in south-north direction. More details on CHRIS-PROBA are given in Barnsley et al. (2004); Cutter and Johns (2005) and on the dedicated website (http://www.chris-proba.org.uk).

4.3 Study site and remote sensing data

The study site is located in the Nismes forest, southern Belgium (50°00' N, 4°34' E). It is characterised by a slightly hilly relief with an altitude varying from 200 m to 350 m above the sea level. The main species are oak (*Quercus* spp.) and Norway spruce (*Picea abies* (L.) Karst), representing more than 90 % of the forested area. The oak stands are usually made of a dominant stage (high forest) of oak trees and an understorey of different deciduous species, namely the hawthorn (*Crataegus sp.*), the hornbeam (*Carpinus betulus* L.) and the hazel (*Corylus avellana* L.). On the other hand, the spruce stands are even-aged and without understorey vegetation, except for the young stands in which shrubs of deciduous species are well developed and compete with the spruce plantation. At the time of the CHRIS data acquisition, all the deciduous species were leafless. The crown coverage in the middle-aged and mature spruce stands was always over 90 % while in one selected oak stand it was about 70 %. The main characteristics of the selected forest stands are reported in table 4.1. The figure 4.2 shows an aerial photograph of oak and spruce stands similar to the ones of the studied area.

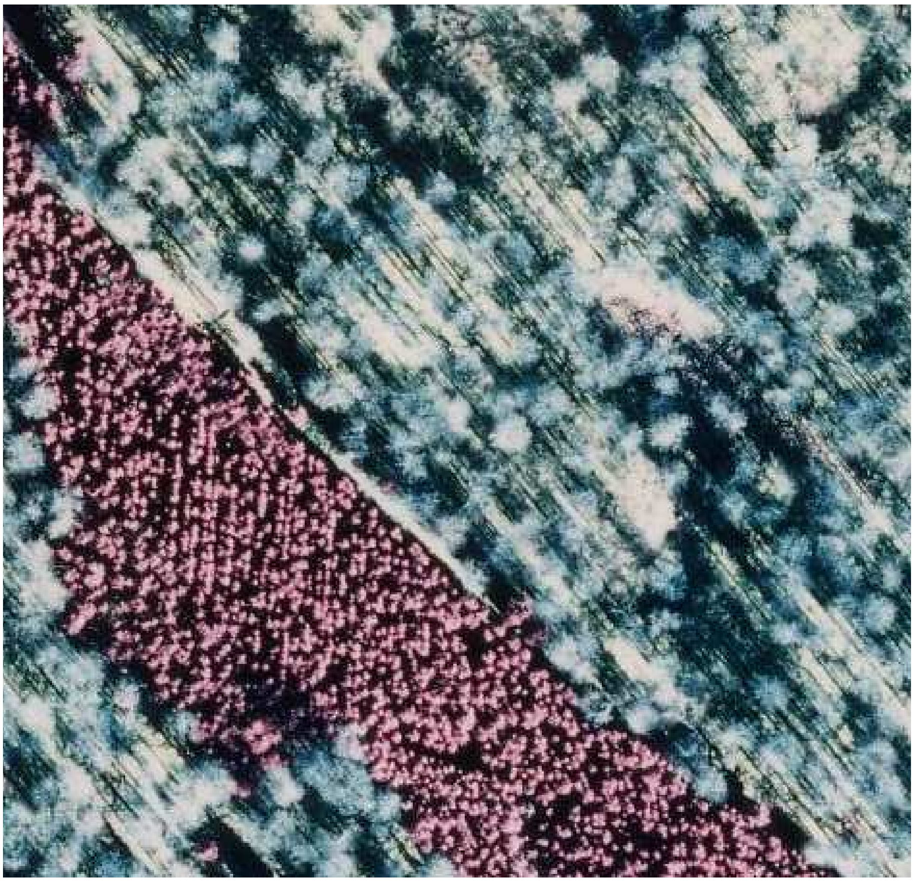

Figure 4.2: An aerial infrared false colour photograph of forest stands similar to ones of the study area. The coniferous appear in red, the deciduous tree crown in grey. Note that the photograph was taken during winter.

Table 4.1: Description of the studied forest types

Code	Main species	Age (years)	Basal area ($m^2.ha^{-1}$)	Density ($N.ha^{-1}$)	Height (m)	Description
CYO	Spruce	10	-	2860	5	Young plantation with open canopy
CME	Spruce	26	42	2140	15	Middle-aged plantation with closed canopy
CMA	Spruce	90	40	360	25	Mature stand with closed canopy
BME	Oak,Birch	-	18	540	20	Middle-aged stand with a regular structure and a closed canopy
BMA	Oak	-	22	250	25	Mature stand with closed canopy, one stage, herbaceous understorey
BMA2	Oak, Birch, Cheesnut	-	15	160	25	Mature stand with open canopy in the upper stage, and understorey made of birch and cheesnut

Table 4.2: Acquisition configuration parameters of the CHRIS images on April 9, 2003.

Fly-by zenith angle (FZA, deg)	+55	+36	0	−36	−55
Viewing zenith angle (θ_r, deg)	51.4	34.6	22.9	36.8	53.0
Viewing azimuth angle (ϕ_r, deg)	32.3	49.9	105.4	157.1	172.4
Solar zenith angle (θ_i, deg)	44.2	44.1	44.0	44.0	43.9
Solar azimuth angle (ϕ_i, deg)	159	160	160	160	161
Satellite altitude (km)	667	665	663	661	658
Time (hh:mn:ss)	10:46:54	10:47:44	10:48:33	10:49:23	10:50:12

The remote sensing data consisted in a set of five hyperspectral images acquired by the CHRIS sensor on 9 April 2003. The site was imaged by laterally pointing with a minimum zenith angle (MZA) of 22°. Thus, the five images were off-nadir. As the telemetry data are not provided to users, the satellite position (azimuth and zenith angles as well as altitude) can be determined with reasonable accuracy using an orbital propagation model and the *Two-Line Elements* (TLE) data. We used for this the WXtrack package (http://www.satsignal.net). Detailed information about the acquisition configuration are reported in table 4.2.

Extracts from the CHRIS images are shown on figure 4.4 as infrared false-colour composites (bands 785 nm, 631 nm and 551 nm in the red, green and blue channels, respectively). A linear saturating contrast enhancement with break points at 2% (Schowengerdt, 1997, p. 204) was applied on each image. The two bottom images (FZA of −36° and −55°) have been acquired in the backward configuration, the three others, in the forward configuration. Note that vegetation, namely forests, is redder in the backward configuration than in the forward as a consequence of relatively higher radiances in the infrared band. The polar plot of the figure 4.4 shows also that the −36° and −55°–FZA images are close to the hotspot configuration.

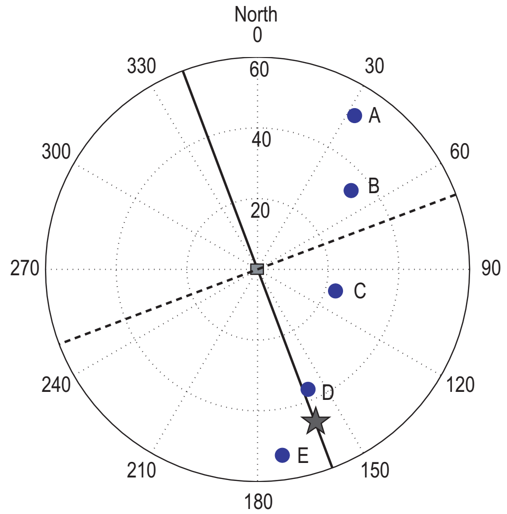

Figure 4.3: Polar plot showing the positions of the satellite (•) and the Sun (⋆) at the image acquisition moment, the principal (—) and perpendicular (- - -) planes. The circular axis represents the azimuth angle and the radial axis represents the zenith angle. Letters A-E show the correspondence with the image extracts shown on figure 4.4.

The images were acquired in the so-called 'chlorophyll' mode, i.e. with the highest spatial resolution, full swath and 18 spectral bands suited to vegetation applications (table 4.3). The images were delivered at 1A-processing level; that is they have been corrected for radiometric calibration only.

4.4 Method

4.4.1 Data processing

The first step of the data processing was to co-register the five images so that to deliver angular profiles. As the 2^{nd} and 4^{th} images

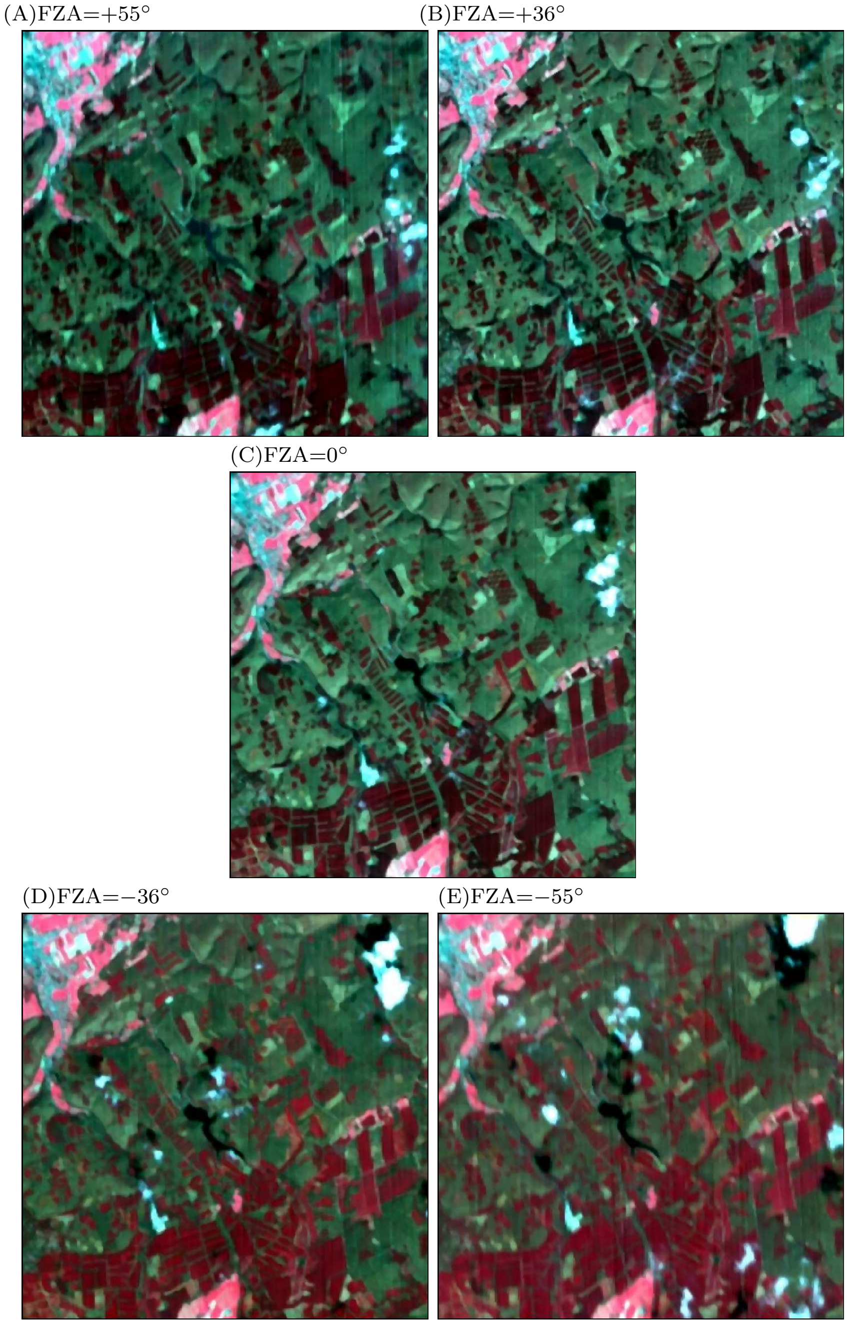

Figure 4.4: Extracts from the CHRIS data displayed as infrared false-colour composites (bands 785 nm, 631 nm and 551 nm in the red, green and blue channels, respectively).

Table 4.3: Spectral bands of the CHRIS images acquired in the so-called "chlorophyll" mode

Band number	Band centre (nm)	Width (nm)	Band number	Band centre (nm)	Width (nm)
C1	489	9	C10	709	6
C2	551	10	C11	716	6
C3	631	9	C12	735	7
C4	672	11	C13	742	7
C5	680	6	C14	748	7
C6	686	6	C15	755	7
C7	691	6	C16	777	7
C8	697	6	C17	785	8
C9	703	6	C18	792	8

In this mode, the nominal nadir spatial resolution was 17 m at an altitude of 556 km, and the swath width was 13 km

in the five image series, i.e. the $+36°$ and $-36°$–FZA images, were acquired in asynchronous scanning mode, they were firstly flipped in order to put them in the same orientation as the three others. Secondly, co-registration of the four far off-nadir images to the nearest-nadir image was performed using a first order polynomial model adjusted from 15 tie points collected on the nearest-nadir image (reference image) and on each of the other four images. Finally, the nearest-nadir image was geometrically corrected using a 2^{nd} order polynomial model adjusted from 16 ground control points. The ground control points were collected from digital colour orthophotographs having a spatial resolution of 0.40 m. The same model was subsequently applied to the four co-registered images.

4.4.2 Angular and spectral signature analysis

The angular and spectral signatures analysis was carried out on the basis of samples taken from six different forest types (table 4.1). The forest stands were selected on flat terrain to avoid topographic effects as we were dealing with multiangular images. The stands had also to be large enough (at least 2 ha) in order to have homogeneous pixels within the stand. A set of five pixels was selected randomly in each stand and constituted the basis of subsequent analysis. The angular and spectral profiles of the six forest types were compared and the effect of the viewing angle was tested by the means of the analysis of variance of the top-of-atmosphere (TOA) radiance. No atmospheric correction was applied as the five images were acquired within a very short time interval (less than 4 minutes). However, the atmosphere path length have influenced the at-sensor recorded radiance by increasing the diffusion and signal attenuation, namely in the visible domain.

In order to separate the directional effects from the spectral signature of a target, Sandmeier and Itten (1999) proposed an anisotropy factor that was calculated by normalizing the reflectance, R, in a specific view direction to the nadir reflectance, R_0, for a given incident irradiance direction (equation 4.1):

$$ANIF(\theta_r, \phi_r; \lambda) = \frac{R(\theta_r, \phi_r; \lambda)}{R_0(\lambda)}, \tag{4.1}$$

where θ_r and ϕ_r are the zenith and azimuth angles of the viewing direction, and λ refers to the wavelength. Since this index is based on the nadir reflectance, its use with space-borne sensor data is constrained by the fact that the required nadir views are not necessarily available from a multiple view angle satellite, such as PROBA. Strub et al. (2002) proposed to normalise the directional reflectance data by the hemispherical reflectance:

$$ANIF_{BHR}(\theta_r, \phi_r; \lambda) = \frac{R(\theta_r, \phi_r; \lambda)}{\frac{1}{\pi}\int_0^{2\pi}\int_0^{\pi/2} R(\theta_r, \phi_r; \lambda)\, cos\theta_r sin\theta_r \, \mathrm{d}\theta_r \mathrm{d}\phi_r}. \tag{4.2}$$

However, the angular sampling remains usually poor, especially for space-borne sensors. The integral in equation 4.2 should therefore be replaced by a discrete approximation. Furthermore, for space-borne sensor data, the view direction sampling is never regular so that the discrete approximation of the integral in equation 4.2 should be replaced by the sum of reflectances over all sampled view directions. Thus, we propose a directional reflectance index (DRI) computed as follows:

$$DRI(\theta_r, \phi_r; \lambda) = \frac{R(\theta_r, \phi_r; \lambda)}{\sum_{\theta_r} \sum_{\phi_r} R(\theta_r, \phi_r; \lambda)}. \tag{4.3}$$

In this study we used the top-of-atmosphere radiances instead of reflectances in equation 4.3. This should not influence the main conclusions since further analyses were done on different spectral bands separately.

4.5 Results

4.5.1 Image registration

Automated processing of multi-angle images requires accurate co-registration, namely an error of less than 1 pixel. In this study, the co-registration of the five images resulted in root mean squared residual errors (RMSE) of 0.71, 0.73, 0.82 and 1.18 pixels for the $+36°$, $-36°$, $+55°$ and $-55°$–FZA images, respectively. The geocoding model gave an RMSE of 0.63 pixels, or approximately 13 m as the pixel size of the nearest-nadir image was 20 m. However, in spite of the RMSE of less than 1 pixel for the first three images, visual checking revealed that the corrected images were not well co-registered. Geometric distortions due to the topography were noticeable and could not be corrected with a simple polynomial model. These results also showed that the co-registration quality diminishes with increasing view zenith angle. The systematic geometric distortions and the topographical-induced distortions are more likely when the satellite is pointing far from the nadir. Furthermore, the influence of the view zenith angle and of the slow-down factor applied to increase integration time is more important in the $\pm55°$–FZA images than in the $\pm36°$–FZA images.

For a perfect co-registration between the five images, a rigorous model that takes into account the actual geometry of observation (satellite attitude and sensor parameters) and the Earth characteristics (geoid-ellipsoid, elevation, projection) is required. Building such a model was however beyond the scope of this study.

4.5.2 Angular and spectral signature analysis

Figures 4.5 and 4.6 show the average radiances of three deciduous stands and three coniferous stands as a function of the FZA and the wavelength. The data have been interpolated for visualisation purposes. The interpolation method is based on a Delaunay triangulation of the data that uses the Qhull algorithm (Barber et al., 1996). The classical spectral signatures of the vegetation were well observed for the coniferous stands while the deciduous stands showed, as expected, low radiance in the near-infrared bands because the images were acquired during winter. Note also the trough around 755 nm which is due to the absorption by the atmospheric oxygen.

For almost all spectral bands, the radiance decreases slightly from the FZA of $+55°$ to $0°$ and increases significantly when the viewing configuration tends towards the hot spot point which is located somewhere between the $-36°$ and $-55°$–FZA configurations. That is also illustrated on figure 4.7 where the six forest types are compared for some selected spectral bands. In the green (551 nm) and red (631 nm) bands, the radiance increase between $-36°$ and $-55°$ keeps high rate while in the red-edge (716 nm) and near-infrared regions (785 nm) there is either a slight increase or even a decrease. The trend in the red-edge and near-infrared regions agrees with the fact that the maximum radiance should be observed in the hot spot configuration (figure 4.4). In the visible region, this trend was hidden by the atmospheric effect.

The figure 4.8 illustrates also that the BRDF effect is spectral dependent. For example, the mature coniferous stand had the lowest radiance values in the near-infrared bands and in the "forward" configuration whereas it had almost equivalent radiance as the middle-aged coniferous stand in the visible bands, whatever was

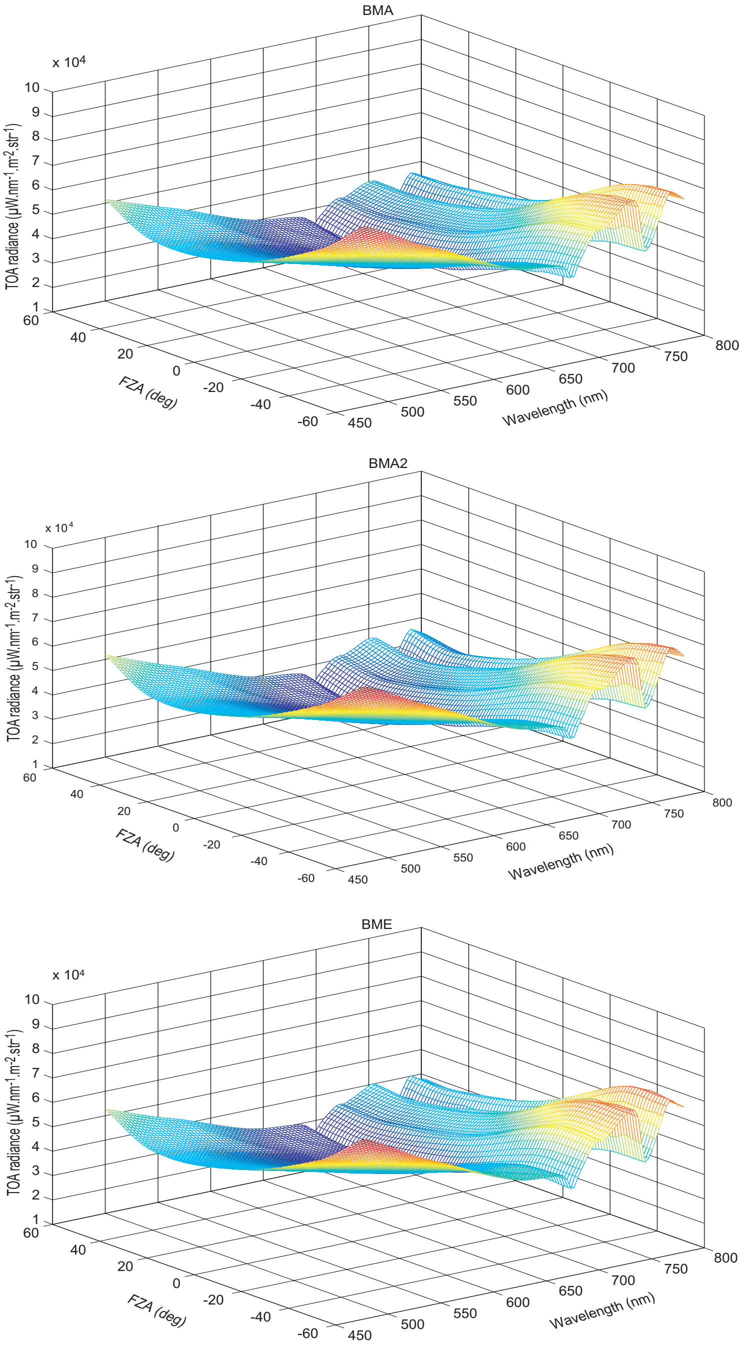

Figure 4.5: Top-of-atmosphere radiance as function of the spectral band wavelength and the fly-by zenith angle for a mature deciduous stand with high density (top), a mature deciduous stand with low density (middle) and a middle-aged deciduous stand (bottom).

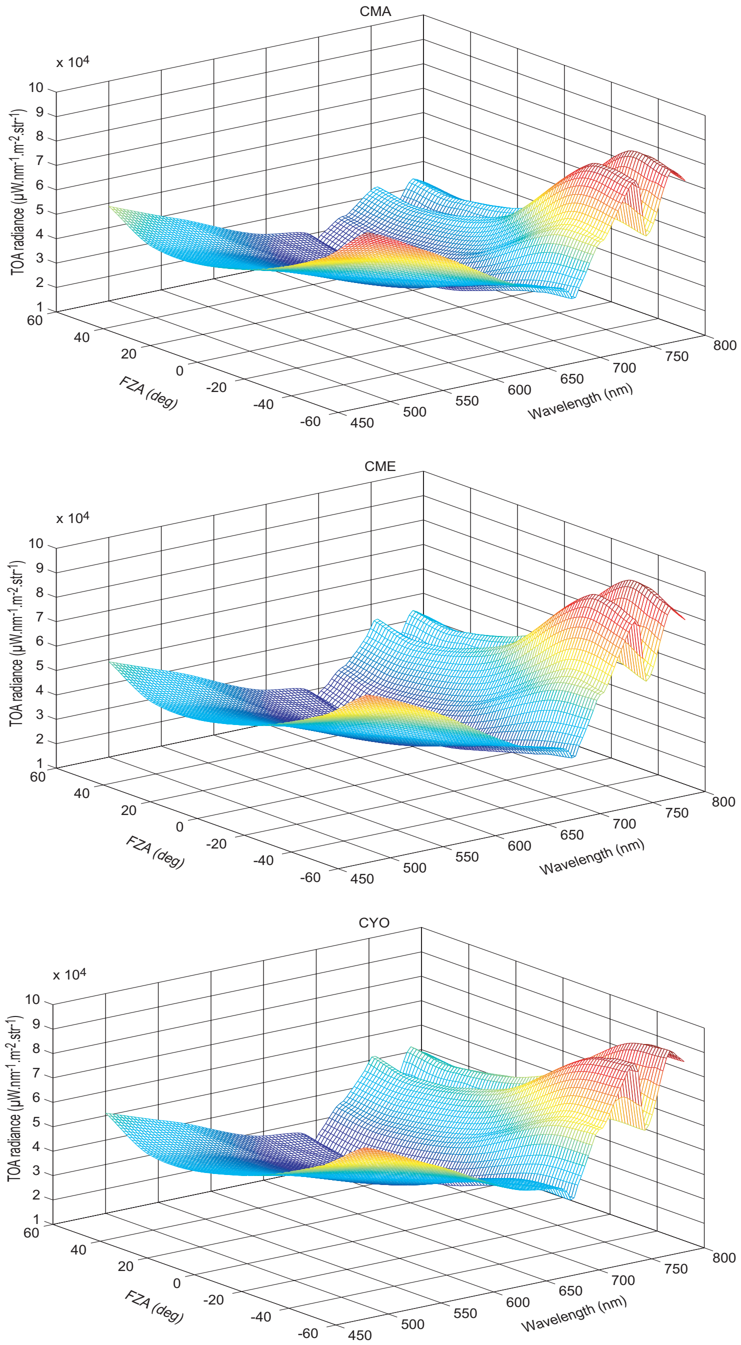

Figure 4.6: Top-of-atmosphere radiance as function of the spectral band wavelength and the fly-by zenith angle for a mature coniferous stand (top), a middle-aged coniferous stand (middle) and a young coniferous stand (bottom).

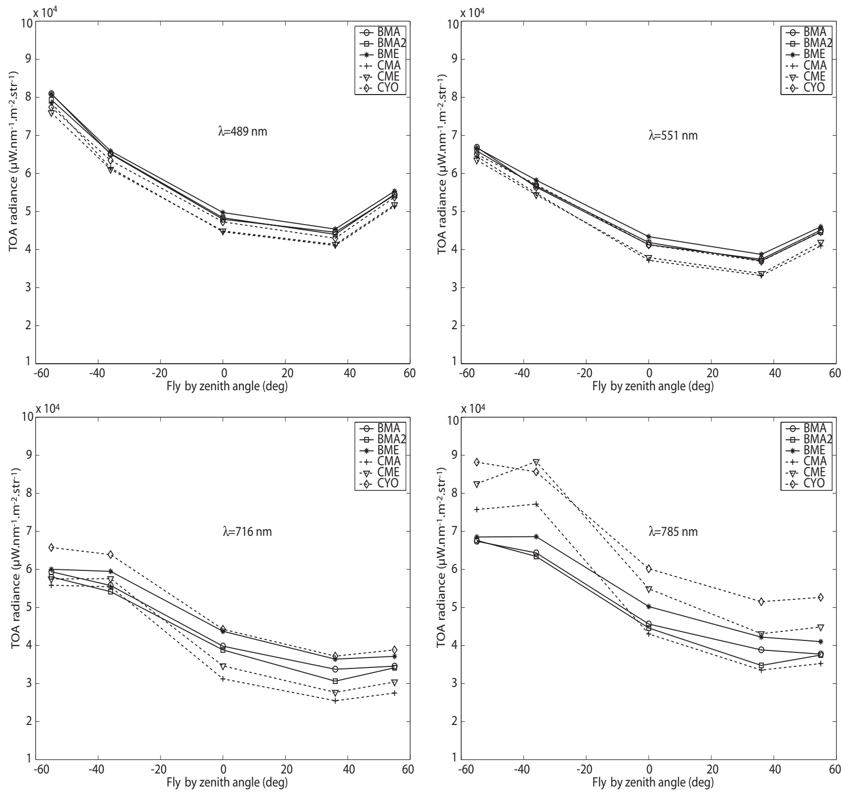

Figure 4.7: Top-of-atmosphere radiance as function of the fly-by zenith angle for different forest stands at four key spectral bands. The forest types acronyms are explained in table 4.1.

the viewing angle.

When looking close into the directional signature of the six forest types as revealed by the anisotropy index on figure 4.9, it appears that the spectral bands in the visible region, and specially the blue and green bands (489 nm and 551 nm), cannot help discriminating the studied forest types. The directional reflectance index computed in the red bands (631 nm and 672 nm) shows clear different trends between the deciduous stands on the one hand, and the mature and middle-aged coniferous stands, on the other hand. But the young coniferous stand has the same signature as the deciduous stands. In the red-edge and near-infrared regions (figure 4.10), it becomes possible to make a distinction between the three deciduous stand types, namely thanks to the $-55°$ and $+36°$–FZA images. The two mature deciduous stands with different stand density could be discriminated using the $+36°$–FZA data in the NIR bands. Such discrimination was not possible with the near-nadir data alone.

The directional anisotropy due to stand structure was more pronounced in the NIR bands than in the visible region bands, perhaps because the visible wavelengths were more affected by the atmospheric diffusion which tends to mask the directional reflection. Nevertheless, the same findings have been reported by de Wasseige and Defourny (2002) on the basis of tropical forest images recorded by the SPOT-HRV sensor. It is worth noting also that in the near-infrared bands, the anisotropy indices of the mature deciduous stand with high tree density and the young coniferous stand were equivalent for all view angles (figure 4.10) whereas the top-of-atmosphere radiances of these stands were very different (figure 4.7). This is an illustration that the directional reflectance index used in this study was well suited for isolating the directional component of the signal related to the stand structure.

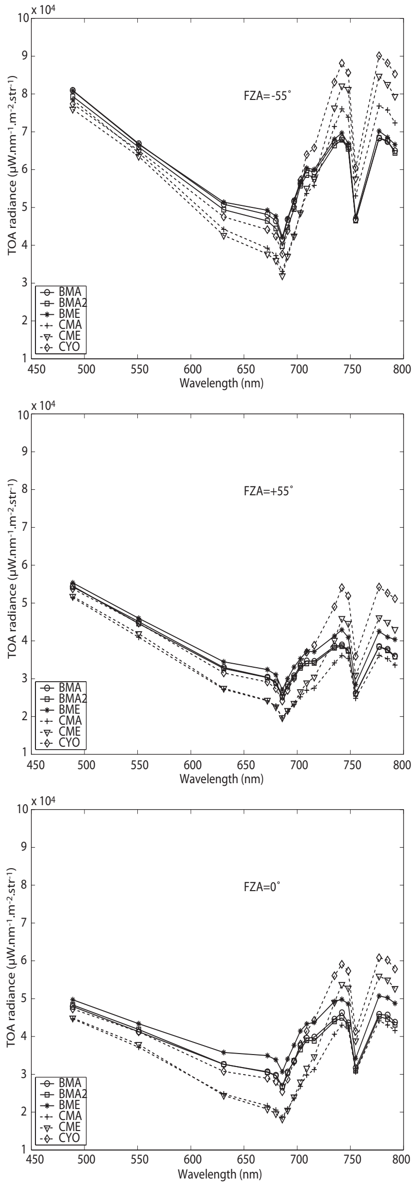

Figure 4.8: Spectral signatures of six forest types at different viewing angles (FZA). The forest types acronyms are explained in table 4.1.

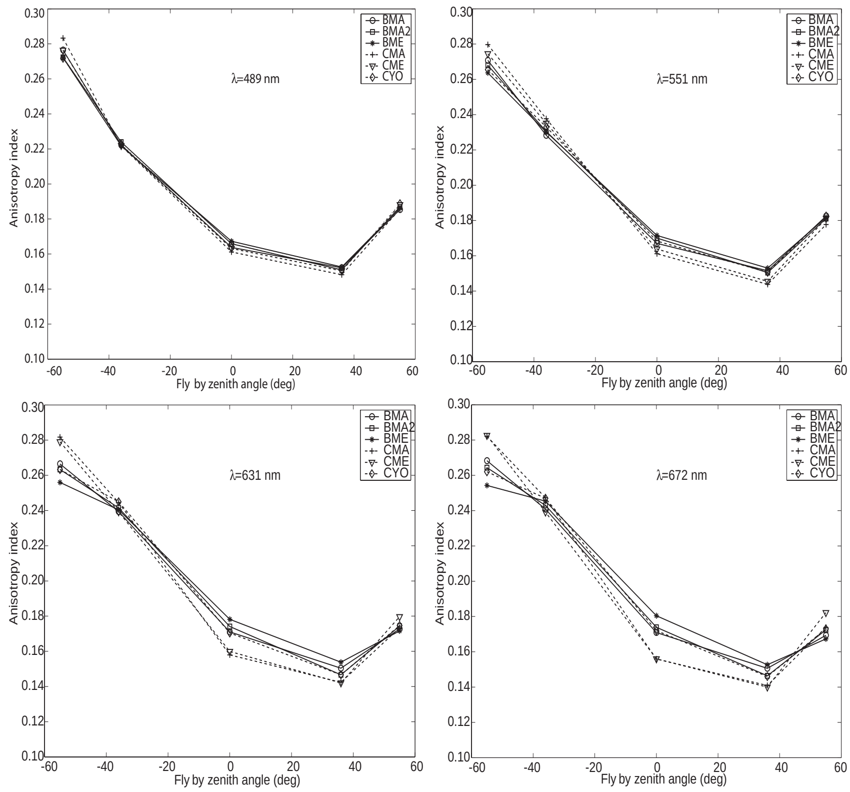

Figure 4.9: Directional radiance index calculated from the blue, green, and red bands. The forest types acronyms are explained in table 4.1.

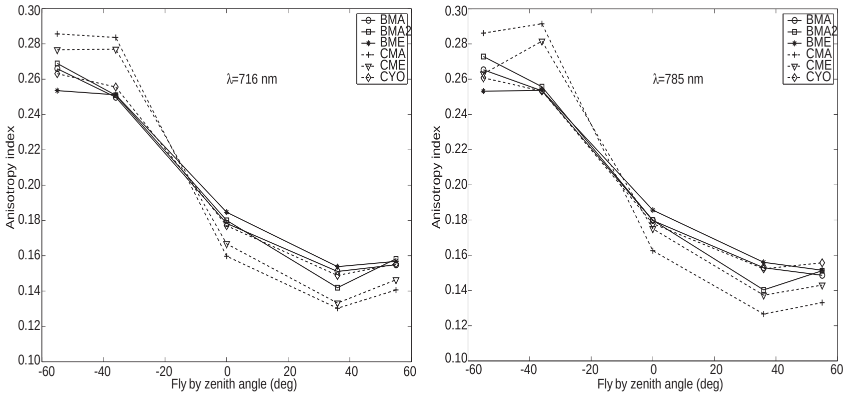

Figure 4.10: Directional radiance index calculated from the red-edge and near-infrared bands. The forest types acronyms are explained in table 4.1.

4.5.3 Statistical investigation of the contribution of the multi-angle data

In order to investigate real contribution of multi-angle data for forest types discrimination, an analysis of variance (ANOVA) was carried out to test the view angle effect on the radiance recorded at the sensor level. The results for selected spectral bands are reported in table 4.4. As expected, for all spectral bands, there is a significant effect of the forest types and of the view angle, either for coniferous stands or deciduous ones. In some spectral bands (489 nm, 551 nm and 742 nm), the interaction between the forest type and the view angle was not significant for deciduous stands. This means, for these spectral bands, that the different deciduous stands do not show differentiated spectral behaviour depending on the view angle. This fact corroborates what was observed on figures 4.9 and 4.10 that the anisotropy index in these spectral bands could not allow discriminating the studied forest types.

When the global effects are found significant, it is necessary to check which means are really significantly different because there were three or more means to compare. This analysis had been carried out by comparing all pairs of means of the interaction effect.

Table 4.4: ANOVA table for the effects of *Forest type*(FT, $df = 2$) and *View angle*(VA, $df = 4$), and their interaction, on the TOA radiance (residual $df = 60$). Figure in bold means that the effect is not significant at $\alpha = 0.01$ level.

		Coniferous		Deciduous	
Wavelength	Effect	F-value	p-value	F-value	p-value
489	FT	74.76	<0.01	16.38	<0.01
	VA	8528.21	<0.01	5602.91	<0.01
	FT × VA	9.00	<0.01	1.89	**0.08**
551	FT	187.38	<0.01	28.03	<0.01
	VA	6623.47	<0.01	4176.41	<0.01
	FT × VA	8.14	<0.01	2.20	**0.04**
631	FT	478.81	<0.01	87.40	<0.01
	VA	2664.01	<0.01	2385.44	<0.01
	FT × VA	7.41	<0.01	2.91	<0.01
672	FT	493.37	<0.01	117.13	<0.01
	VA	1456.55	<0.01	1591.61	<0.01
	FT × VA	7.22	<0.01	4.09	<0.01
716	FT	1120.77	<0.01	123.62	<0.01
	VA	4396.20	<0.01	2342.27	<0.01
	FT × VA	4.84	<0.01	2.20	<0.01
742	FT	856.35	<0.01	80.29	<0.01
	VA	3981.63	<0.01	2114.42	<0.01
	FT × VA	21.04	<0.01	2.70	**0.01**
755	FT	765.55	<0.01	76.50	<0.01
	VA	4233.43	<0.01	2366.21	<0.01
	FT × VA	25.46	<0.01	4.42	<0.01
785	FT	1261.97	<0.01	80.39	<0.01
	VA	5567.10	<0.01	1771.06	<0.01
	FT × VA	30.53	<0.01	5.22	<0.01

We were indeed interested in the interaction effect which allowed to assess the contribution of the multi-angle data in discriminating forest types. This contribution becomes critical for forest types which are not separable with one-angle data, namely the near-nadir image. Thus, the results reported in tables 4.5 and 4.6 concern comparison between mean radiance measured with the same viewing angle for the deciduous and the coniferous forest stands, respectively. There were 15 means to compare per spectral band for either deciduous stands or coniferous stands. In order to control the 1 type error rate, the Tukey method (Duncan, 1955) was used.

For the coniferous forest types (table 4.6), the results show that the pairwise comparisons of radiance means involving the red-edge and near infra-red bands (716 to 785 nm) were highly significant in most of the cases. In two cases, i.e. comparison between the mature and middle-aged stand in the $-55°$ image at 716 nm wavelength, and between the mature and young stand in the $-36°$ image at 742 nm wavelength, the test was not significant at 5% level. It should be underlined that on the basis of single view data, say the near-nadir image, the radiance means were significantly different for several spectral bands. That is the directional information provided by the multiple view angle data was not absolutely necessary in discriminating the studied coniferous forest types.

On the other hand, when we consider the deciduous forest types (table 4.5), not a single view image at any wavelength showed significantly different radiance means for all pairwise forest types comparison. In many cases, the radiance means of the mature and the middle-aged stands were found significantly different, for example in the near-nadir image at the red, red-edge and near-infrared wavelengths. However, the comparison test of the radiance means between the low density and the high density mature stands was significant only in the $+36°$ image at the red-edge and near-infrared wavelengths. The multiple view angle data were therefore essential in order to discriminate these forest types.

Table 4.5: Pairwise comparison of the mean radiance to assess the contribution of the view angle effect. Results (p-values) of the Tukey's test for the deciduous forest stands. The forest type acronyms are explained in table 4.1.

Wave-length	Forest types	Fly-by zenith angle				
		−55°	−36°	0°	+36°	+55°
489	BMA-BMA2	0.08	1.00	1.00	1.00	1.00
	BMA-BME	1.00	0.92	0.03	0.91	0.62
	BMA2-BME	0.11	0.99	0.21	0.22	0.89
551	BMA-BMA2	0.72	1.00	0.99	1.00	1.00
	BMA-BME	1.00	0.01	<0.01	0.24	0.80
	BMA2-BME	0.92	0.08	0.06	0.03	0.14
631	BMA-BMA2	0.16	1.00	1.00	0.42	1.00
	BMA-BME	1.00	<0.01	<0.01	<0.01	0.11
	BMA2-BME	0.01	<0.01	<0.01	<0.01	0.03
672	BMA-BMA2	0.17	1.00	1.00	0.56	1.00
	BMA-BME	0.79	<0.01	<0.01	<0.01	0.04
	BMA2-BME	<0.01	<0.01	<0.01	<0.01	0.02
716	BMA-BMA2	0.62	0.32	0.94	<0.01	1.00
	BMA-BME	1.00	<0.01	<0.01	<0.01	<0.01
	BMA2-BME	0.09	<0.01	<0.01	<0.01	<0.01
742	BMA-BMA2	1.00	0.51	0.88	0.01	1.00
	BMA-BME	0.81	0.23	<0.01	0.03	0.01
	BMA2-BME	0.51	<0.01	<0.01	<0.01	<0.01
755	BMA-BMA2	1.00	0.98	0.98	<0.01	1.00
	BMA-BME	0.98	0.08	<0.01	0.08	<0.01
	BMA2-BME	0.80	<0.01	<0.01	<0.01	<0.01
785	BMA-BMA2	1.00	1.00	0.99	<0.01	1.00
	BMA-BME	0.99	<0.01	<0.01	0.01	0.02
	BMA2-BME	1.00	<0.01	<0.01	<0.01	<0.01

Table 4.6: Pairwise comparison of the mean radiance to assess the contribution of the view angle effect. Results (p-values) of the Tukey's test for the coniferous forest stands. The forest type acronyms are explained in table 4.1.

Wave-	Forest types	Fly-by zenith angle				
length		−55°	−36°	0°	+36°	+55°
489	CMA-CME	<0.01	1.00	1.00	1.00	1.00
	CMA-CYO	0.03	<0.01	<0.01	<0.01	<0.01
	CME-CYO	0.26	<0.01	<0.01	<0.01	<0.01
551	CMA-CME	0.35	1.00	0.82	1.00	0.47
	CMA-CYO	0.01	<0.01	<0.01	<0.01	<0.01
	CME-CYO	0.98	<0.01	<0.01	<0.01	<0.01
631	CMA-CME	0.03	<0.01	1.00	1.00	1.00
	CMA-CYO	<0.01	<0.01	<0.01	<0.01	<0.01
	CME-CYO	<0.01	<0.01	<0.01	<0.01	<0.01
672	CMA-CME	0.21	<0.01	0.94	0.91	1.00
	CMA-CYO	<0.01	<0.01	<0.01	<0.01	<0.01
	CME-CYO	<0.01	<0.01	<0.01	<0.01	<0.01
716	CMA-CME	0.17	0.02	<0.01	0.01	<0.01
	CMA-CYO	<0.01	<0.01	<0.01	<0.01	<0.01
	CME-CYO	<0.01	<0.01	<0.01	<0.01	<0.01
742	CMA-CME	<0.01	<0.01	<0.01	<0.01	<0.01
	CMA-CYO	<0.01	0.41	<0.01	<0.01	<0.01
	CME-CYO	<0.01	<0.01	<0.01	<0.01	<0.01
755	CMA-CME	<0.01	<0.01	<0.01	<0.01	<0.01
	CMA-CYO	<0.01	0.01	<0.01	<0.01	<0.01
	CME-CYO	<0.01	<0.01	<0.01	<0.01	<0.01
785	CMA-CME	<0.01	<0.01	<0.01	<0.01	<0.01
	CMA-CYO	<0.01	0.01	<0.01	<0.01	<0.01
	CME-CYO	<0.01	<0.01	<0.01	<0.01	<0.01

4.6 Discussion

In the previous section, it has been shown that the distinction between two deciduous stands with different tree densities was possible only in the image acquired with a FZA of +36°. How can we explain this phenomenon?

Considering figure 4.4, we can see that the +36°–FZA image configuration was the closest to the plane perpendicular to the principal plane. As the images were taken in winter, the tree shadows cast to the understorey alternated with sunlit zones of the understorey (figure 4.2). Thus the proportion of shadowed understorey that was sensed by the satellite explained the difference in the reflected radiance of the two forest types. The stand with low density had more proportion of shadowed understorey than the high density stand due to the presence of shrubs in the sub-stage of the stand with low density. This conclusion is supported by the fact that in almost all wavelengths and all view angles, the reflected radiance of the young deciduous stand is higher than the radiance of the mature high density stands, which is also higher than or equal to the radiance of the mature low density stand (figure 4.7). The understorey contributed significantly to the total radiance of the stand. That is why for example the leaveless stands and the young coniferous stand showed less pronounced BRDF effects than the other coniferous stands.

According to Sandmeier et al. (1998), if the soil/background influences are negligible, the BRDF effects are most pronounced in erectophile canopies and are reduced in planophile canopies. In the case of this study, the deciduous stands and the young coniferous stands had an erectophile architecture while the other two coniferous stands had a rather planophile architecture.

The shadowing effect discussed above is the main cause of the directional anisotropy of reflected radiance over vegetation canopies where scattering elements are much larger than the wavelength, as shown by Hapke et al. (1996) in studying the cause of the hot spot in vegetation canopies. The directional anisotropy of the reflected radiance was found more pronounced in the forest stand with closed canopies, namely the mature and middle-aged coniferous stands (figure 4.10). There are two sources of that effect.

Firstly, the shadow-hiding mechanism responsible of the hot spot effect was more evident in the coniferous stands with closed canopies than in the deciduous stands, whose canopies were made only with boles without leaves, and in the young coniferous stand, whose canopy was not yet closed (figures 4.9 and 4.10). Indeed, in the two last cases, there were a large contribution of the background to the total radiance. The forward scattering is more likely to occur on such a background, raising the radiance in the forward direction.

Secondly, multiple scattering of the radiation by the sunlit background and also by the canopy elements (boles and needles) is more important in open canopies than in closed canopies. There is more diffuse radiance in the "shadow" side when there is a large part of sunlit background.

The fact that the directional reflectance index of a young coniferous stand was found equivalent to the one of a mature deciduous stand brings a new information in the understanding of the relationship between physical characteristics of a forest and its BRDF captured by a high spatial resolution sensor such as CHRIS. It appears that the horizontal arrangement of the trees and the stand density influence more the directional component of the radiance than the tree height and diameter.

It has been observed also that the directional effect due to vegetation cover was more contrasted in the near-infrared bands than in the visible bands. This observation does not agree with the one made on the basis of ground measurements, where the directional effects were more contrasted in the high-absorbing spectral bands (blue and red) than in the low-absorbing bands, i.e. the green and near-infrared bands (Kimes, 1983; Sandmeier and Itten, 1999; Deering et al., 1999). This was due to atmospheric effect which are more pronounced in the short wavelengths of the visible region than in the longer wavelengths of the near-infrared region. Indeed, there was no difference in the anisotropy index trends of the blue and red bands on one hand and the green band on the other hand.

The methods of atmospheric correction usually applied do not take into account the land cover type at a level as detailed as the forest stand. Thus, the near-infrared bands seem to be the most interesting in discriminating the forest stand type when using multi-angle data acquired by space-borne sensors.

4.7 Conclusion

The contribution of the multiple view-angle remote sensing data to forest stand characterization has been investigated with emphasis on assessment of the specific contribution of the angular information compared to traditional spectral signature.

The six forest types studied here showed different directional signatures (revealed namely by the anisotropy index) but most of them could be discriminated on the basis of the near-nadir spectral signature alone. The means of reflected radiances of this near-nadir image at the red-edge and near-infrared wavelengths were found significantly different for all pairwise comparisons within either coniferous or deciduous stands, except for the comparison between the mature deciduous stands. Their mean radiances were significantly different in the images acquired with a FZA of +36°, i.e. when the sensor was close to the plane perpendicular to the principal plane. It appeared therefore that, on the one hand, the contribution of the multiple view angle is important in differentiating some particular forest types in relation to their structural characteristics, and on the other hand, that the spectral effects are the main driving factor in discriminating most forest types. Spectral data from the +36°-FZA image were sufficient to discriminate the six forest types that have been studied. With respect to this, the possibility to choose the viewing angle was more important than acquiring images with several viewing angles systematically. But for this selection, we need clear understanding of the directional behaviour of the data recorded by space-borne sensors at the stand level.

In this study, we used images acquired during winter while, traditionally, the forest remote sensing studies used images taken during the growing season. The images of deciduous stands acquired during winter have been found particularly interesting to understand the mechanism of the directional anisotropy. The proportion of sensed shadow, cast to the background, was found to be the main cause of the anisotropy in such images. It was therefore possible to make distinction between two mature deciduous forest stands having different tree densities.